AIP | The Journal of Chemical Physics

Thermodynamic precursors, liquid-liquid transitions, dynamic and topological anomalies in densified liquid germania

F. Pacaud and M. Micoulaut

Citation: The Journal of Chemical Physics **143**, 064502 (2015); doi: 10.1063/1.4927707
View online: http://dx.doi.org/10.1063/1.4927707
View Table of Contents: http://scitation.aip.org/content/aip/journal/jcp/143/6?ver=pdfcov
Published by the AIP Publishing

Thermodynamic precursors, liquid-liquid transitions, dynamic and topological anomalies in densified liquid germania

F. Pacaud and M. Micoulaut
Laboratoire de Physique Théorique de la Matière Condensée, Paris Sorbonne Universités, UPMC, 4 Place Jussieu, F-75252 Paris Cedex 05, France

(Received 5 February 2015; accepted 21 July 2015; published online 10 August 2015)

The thermodynamic, dynamic, structural, and rigidity properties of densified liquid germania (GeO_2) have been investigated using classical molecular dynamics simulation. We construct from a thermodynamic framework an analytical equation of state for the liquid allowing the possible detection of thermodynamic precursors (extrema of the derivatives of the free energy), which usually indicate the possibility of a liquid-liquid transition. It is found that for the present germania system, such precursors and the possible underlying liquid-liquid transition are hidden by the slowing down of the dynamics with decreasing temperature. In this respect, germania behaves quite differently when compared to parent tetrahedral systems such as silica or water. We then detect a diffusivity anomaly (a maximum of diffusion with changing density/volume) that is strongly correlated with changes in coordinated species, and the softening of bond-bending (BB) topological constraints that decrease the liquid rigidity and enhance transport. The diffusivity anomaly is finally substantiated from a Rosenfeld-type scaling law linked to the pair correlation entropy, and to structural relaxation. © *2015 AIP Publishing LLC.* [http://dx.doi.org/10.1063/1.4927707]

I. INTRODUCTION

Germanium dioxide (GeO_2) and silicon dioxide (SiO_2) are chemical analogues which share a certain number of similarities, the most obvious one being their common local sp^3 tetrahedral geometry at ambient conditions, which changes with increasing pressure P.[1] At elevated pressures, the structure of both materials becomes indeed octahedral[2–5] and an important body of research has been devoted to the understanding of such changes which are accompanied by changes in thermal, dynamic,[6] and vibrational properties.[7] The presence of two possible local geometries can actually be simply understood from the important difference in density (4.28 g/cm^3 against 6.25 g/cm^3) of the corresponding low tetrahedral (α-quartz) and high pressure (rutile, octahedral) crystalline polymorphs.[1] In GeO_2 crystals, transformations under pressure are rather well documented because the known phase diagram is rather simple,[8] at least when it is compared to silica. Because of the lack of translational symmetry, much less is known in the liquid state although it is now well established that important structural changes also take place,[9] some of them being related to a possible liquid-liquid transition (LLT).[10] At ambient temperature, experiments[2–5] and simulation work[9,11–13] have provided evidence that germania (i.e., amorphous GeO_2) undergoes changes with increase of the pressure, which manifest both at the local and intermediate range order.[14] When compared to silica, it has been found that GeO_2 displays an increased sensitivity to pressure so that it undergoes pressure induced changes at much lower pressures than in crystalline or amorphous SiO_2 analogues.

However, the easy decomposition of liquid GeO_2 at high pressure and temperature into elementary germanium and oxygen[15] prevents unfortunately from a systematic experimental study of the (P,T) phase diagram. A tentative one has been proposed[10] which shows a flattening of the crystallization curve at ≃2-4 GPa, indicative of a considerable densification of the melt. It is has been stated that this may be related to a diffuse transformation from α-quartz to rutile-like polymorphs. Once the crystallization is bypassed upon cooling, a critical point (T_c) is expected, similarly to other liquid substances. Below T_c, the liquid is then supposed to develop a mixing of a low density liquid (LDL) and high density liquid (HDL), separated by a transition line.[10,16] Corresponding glass transition temperatures are expected to be different. At low temperature, amorphous-amorphous transformations (AAT) are detected from the time evolution of the volume which manifest by irreversible relaxation in the region 3-4 GPa, associated with coordination changes and important compressibility variations.[17]

In numerical studies of other tetrahedral systems (water and silica), it has been possible to determine such a critical temperature T_c at which the LLT onsets,[18,19] as well as characteristic patterns of "*thermodynamic precursors*"[20–22] which display an anomalous behavior (density and compressibility maximum) for $T > T_c$. These anomalies are usually correlated with changes in the local structure of the liquid, involving higher coordinated species which can have two types of local arrangements. In liquid germania however, such numerical studies have not been considered. This is the purpose of the present paper, and the output may be particularly interesting since it is well-known that GeO_2 displays typical temperatures that are more accessible than the silica analogue, i.e., one has $T_m = 1388$ K and $T_g = 850$ K,[23] allowing for a possible study for such changes in the liquid and the supercooled state, also

facilitated by an increased sensitivity of structural changes induced by pressure.[2–5]

It should be emphasized that there is no general agreement on the link between such precursors, for instance, a "temperature of maximum density" (TMD observed in, e.g., silica[24]), and the LLT. Alternative frameworks for the liquid anomalies (and eventually LLT) have been developed more recently (for a review on water, see Refs. 25 and 26), and these involve either secondary critical points[27,28] or the decoupling of the atomic interactions into strong/weak bonds[29] that may be also orientation-dependent.[30] In a series of papers devoted to tetrahedral liquids,[31–34] several authors have suggested that the excess entropy S_e may be responsible for the observed anomalies in thermodynamic, structural, and dynamic properties in relationship with LLTs. These anomalies are thought to result from the presence of two possible structures reminiscent of a high and low density local order, and which can be quantified from a Rosenfeld-type scaling[35] showing that transport properties behave as $\exp[\alpha S_e]$. Similarly, using a two-state model for thermodynamics of LLT, Holten and Anisimov[36] have also detected the role played by entropy upon increasing pressure, which ultimately controls the critical temperature of the LLT through the equilibrium constant ruling the two-state liquids.

Given the similar structure and tetrahedral to octahedral conversion under pressure, it is to be expected that GeO_2 displays polyamorphism or polyamorphic transitions in very much the same fashion as in water,[10] silica, or even other materials covering a wide range of chemical bonding type. For water, it has been proposed that the observed polyamorphism is the sub-T_g extrapolation of the LLT line. More generally, these transitions in the amorphous phase seem indeed to map onto underlying density- or entropy-driven LLT taking place at higher temperature, and such phenomena can be followed only through an exhaustive numerical study of state responses to changes in pressure and temperature. It is also important to mention that such transitions bear some similarities with those driven by changes in the chemical composition which lead to immiscible melts. These are later well documented in silicates and are usually characterized using classical thermodynamics.

Here, we build on an approach that has been developed by Sciortino and co-workers.[37] Using extensive MD simulations, we establish an equation of state for the liquid at various (P,T,V) conditions by using a classical thermodynamic framework. This allows establishing these "*thermodynamic precursors*" to eventually locate a critical point ($T_c \simeq 500$ K). In sharp contrast with silica and water, we find that the temperature T_c is at a temperature which is lower than the glass transition temperature. As a result, the possible detection of such thermodynamic precursors (and the potentially underlying LLT) is hidden by the slowing down of the relaxation and might not be accessible from experiments. In this respect, the present results seem to bear similarities with immiscibility domains in potassium silicates[38] for which the spinodal line is also found at $T < T_g$.

Changes in dynamic properties are furthermore analyzed in the liquid as a function of both volume and temperature and reveal not only diffusivity extrema but also anomalies in corresponding activation energies that highlight the fact that the relaxation dynamics is anomalous in selected volume ranges. These extrema are linked with pair correlation entropy extrema, and previous results for germania are recovered in the present contribution. However, we also establish a link between such transport anomalies and the stiffening of the network structure. Using topological constraints, we establish a volume-temperature rigidity phase diagram, and it is found that bond-bending constraints progressively soften with the tetrahedral to octahedral conversion, while the number of bond-stretching (BS) constraints increases with pressure, leading on the overall to a complex (V,T) phase diagram for rigidity. This underscores the existence of liquids able to adapt their angular motion under increasing stress/pressure.

The article is organized as follows. Section II describes the interaction potential and simulation details. Section III is devoted to the phase diagram for liquid germania and the search for the thermodynamic precursors, which are determined from the equation of state of the numerical thermodynamic data. In Section IV, we calculate the number of topological constraints that lead to the rigidity phase diagram, which is compared to the diffusivity of the densified liquids. Finally, Section V summarizes our findings and brings up some conclusions.

II. SIMULATION DETAILS

272 data points in the (P,T,V) phase diagram have been obtained from trajectories that have been accumulated in the NVE ensemble from 20 ps to over 20 ns, depending on the thermodynamic conditions (the lower the temperature, the longer the runs). The isochores of the lowest temperature (900 K) have been accumulated for 25 ns. Equations of motion have been integrated using a leapfrog Verlet algorithm with a time step of 2 fs. The GeO_2 system is composed of 512 oxygen atoms and 256 germanium atoms interacting via an Oeffner and Elliott (OE) potential[7] given by

$$V_{ij} = \frac{q_i q_j}{r} + A_{ij} \exp[-B_{ij} r] - \frac{C_{ij}}{r} \tag{1}$$

which contains a pairwise Born-Mayer repulsion and an attractive term for the O–O and Ge–O interactions plus a Coulomb interaction with fractional charges, the latter being handled with an Ewald sum, whereas the Ge–Ge potential part contains only a Coulomb interaction. This potential has been fitted to account for the vibrational and structural properties of crystalline GeO_2 and has been used, in particular, to investigate the stability of the crystalline α quartz-like and octahedral rutile-like phases.[7] In the glassy state, it yields an interesting agreement with the experimental density[39] (2.66 g/cm^3) at ambient pressure (2.70 g/cm^3). Recently, the OE potential has been used for the study of structural and thermal properties of liquid GeO_2 which have been found to reproduce not only reasonably well experimental measurements on pair distribution functions or structure factors[9,11] but also enthalpy data of the supercooled liquid.

The initial configuration has been started at a temperature of 6000 K. Densification has been achieved by steps at this temperature prior to a step-like decrease of the temperature allowing for a complete investigation of the thermodynamic diagram in (T,V,P). Ten steps ranging from 6000 K to 1500 K

separated by 500 K have been investigated. Additional isotherms (1400 K, 1200 K, 1100 K, and 900 K) have been also considered. Note that separate low temperature isotherms were chosen for the study of the structural changes in the region where the thermodynamic precursors are being found (see below). Chosen volumes range from 0.20 to 0.37 cm^3/g, the glass density at ambient pressure being $\rho = 2.70$ g/cm^3, and corresponding to the upper boundary of the volume range ($V_g = 0.37$ cm^3/g). It should be stressed that in contrast to liquid silica,[40] no additional repulsion term was necessary in order to avoid a collapse at high temperature and high density due to spurious effects arising from a too attractive O–O interaction.

For completeness, we mention that alternative interaction potentials do exist in the literature, and these have served to describe either the crystalline phases of GeO_2[41] or amorphous germania.[42] Most of these potentials have the form of Eq. (1) although alternative (Morse)[42] or polarizable ion potentials[12] have been proposed to account for either liquid/amorphous germania, or even germanates.

III. SEARCHING THERMODYNAMIC PRECURSORS

Thermodynamic precursors to a LLT have been detected in silica[37] and water[19] from computer simulations using a classical thermodynamics framework. Several thermodynamic properties were derived from an analytical equation of state which was computed from the total energy. We follow exactly the same path, and remind for the reader's convenience the steps that led to the final results for silica,[37] now applied on liquid densified GeO_2.

A. Temperature dependence of the potential energy

Using the MD thermodynamic data points, we start by building a continuous form for the equation of state of the liquid. First, we derive an isochoric temperature dependence for the potential energy $U(T,V)$ and check that it scales as $T^{3/5}$, a behavior that corresponds to a functional dependence valid in simple, dense, and cold liquids.[43] Specifically, we fit our data to the form

$$U(T,V) = 27\left[a(V) + b(V)T^{3/5}\right], \qquad (2)$$

where $a(V)$ and $b(V)$ are polynomial functions. To check the validity of Eq. (2), we represent the simulated energy $U(T,V)$ of germania in a plot of $U(T,V)$ versus $T^{3/5}$ (Figure 1) for different isochores. We immediately note that the $U(T^{3/5})$ dependence is satisfied for all isochores. A linear fit of the energy U reproduces very well the simulation data and allows us to extract the parameters $a(V)$ and $b(V)$ appearing in Eq. (2). A small deviation with respect to Eq. (2) sets in at high temperatures for large volumes (e.g., $V = 0.37$ cm^3/g), i.e., for temperature and density/volume ranges which do not correspond to the thermodynamic conditions at which Eq. (2) is supposed to be valid.[43] At low temperature, the deviation of $U(T,V)$ with respect to its linear behavior in $T^{3/5}$ at higher T is an indication of the progressive departure from an equilibrated liquid (gray zone in Fig. 1), and signals the onset of off-equilibrium, as also obtained from other selected densities.[9]

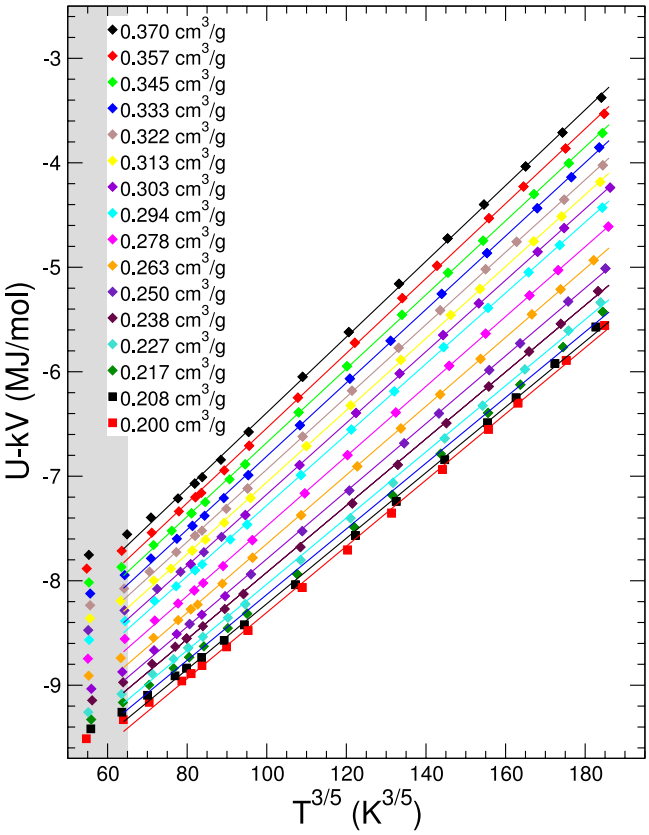

FIG. 1. Behavior of the energy U(T,V) of germania represented as a function of $T^{3/5}$ for several isochores. Symbols are the data points obtained from MD simulations, while the straight lines represent fits using Eq. (2). For clarity, each isochore has been shifted by a quantity kV with k = 10 (g MJ/(cm^3/mol)). The gray zone indicates the glass transition region.

B. Equation of state from free energy

Having established the temperature dependence of the potential energy $U(T,V)$, the parameters $a(V)$ and $b(V)$ can be extracted from Equation (2), and these are now plotted in Figure 2 as a function of the volume V. We note that the V

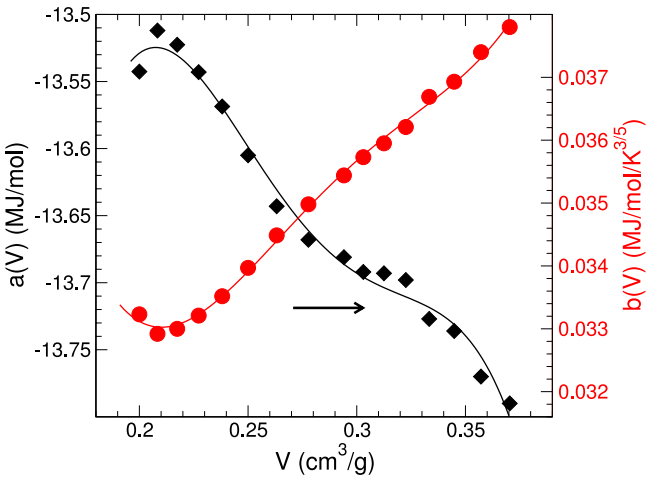

FIG. 2. Behavior of the fitted functions $a(V)$ (black symbols) and $b(V)$ (red symbols, right axis) extracted from the fit of the data represented in Fig. 1, using Equation (2). Data are fitted with a fourth order polynomial in V whose parameters are given in Table I (solid lines).

TABLE I. Fitted coefficients α_n, β_n, and γ_n of the V dependence of $a(V)$ and $b(V)$, and the density dependence of the pressure at $T_0 = 4000$ K. The units of α_n, β_n, and γ_n are those which lead to units in MJ/mol, (MJ/mol)/T$^{3/5}$, and GPa for $a(V)$, $b(V)$, and P, respectively, the volume V and the density ρ being given in cm^3/g and g/cm^3, respectively.

n	α_n	β_n	γ_n
0	−27.874	0.181 89	93.622 9
1	215.15	−2.156 8	−128.955
2	−1180.10	11.388	70.501 9
3	2808.10	−26.027	−19.168 1
4	−2465.80	22.051	2.596 38
5			−0.134 279

dependence of $a(V)$ gives an estimate of Helmholtz free energy that corresponds to the energy $U(T,V)$ at zero temperature.

Fourth order polynomials are used to fit $a(V)$ and $b(V)$, given by $a(V) = \sum_{n=0}^{4} \alpha_n V^n$ and $b(V) = \sum_{n=0}^{4} \beta_n V^n$, the coefficients α_n and β_n being listed Table I. Furthermore, the internal energy E is then given by

$$E(T,V) = a(V) + b(V)T^{3/5} + \frac{9}{2}RT, \tag{3}$$

with R the gas constant, and the added extra term corresponds to the kinetic energy $\frac{9}{2}RT$.

From the established behavior of the energy $E(T,V)$ of liquid germania (Eq. (3)), we now follow a standard framework of classical thermodynamics. The equation of state can be determined from the free energy $F(T,V)$ using the Maxwell equation

$$P(V,T) = -\left(\frac{\partial F}{\partial V}\right)_T, \tag{4}$$

while the free energy $F(T,V)$ is obtained from the equation $F(T,V) = E(T,V) - TS(T,V)$. We use thermodynamic integration in order to determine the entropy $S(T,V)$ which can be separated into a contribution of isothermal ΔS_T and isochoric ΔS_V transformations, and can be written as

$$S(T,V) = S(T_0,V_0) + \Delta S_T + \Delta S_V, \tag{5}$$

$S(T_0,V_0)$ being the entropy of a reference state that we chose to be $T_0 = 4000$ K and $V_0 = 0.2$ cm^3/g. The entropy contribution $\Delta S_T = S(T_0,V) - S(T_0,V_0)$ along an isotherm is computed using

$$\Delta F = \Delta E - T_0 \Delta S_T, \tag{6}$$

with

$$\Delta F = F(T_0,V) - F(T_0,V_0) \tag{7}$$

and

$$\Delta E = E(T_0,V) - E(T_0,V_0), \tag{8}$$

the latter being calculated from Equation (3). It can be furthermore noticed that ΔF is essentially due to a volume change along an isotherm $T = T_0$, which can be determined from an isothermal integration of $dF = -PdV$ leading to

$$\Delta F = -\int_{V_0}^{V} P(T_0,V')dV'. \tag{9}$$

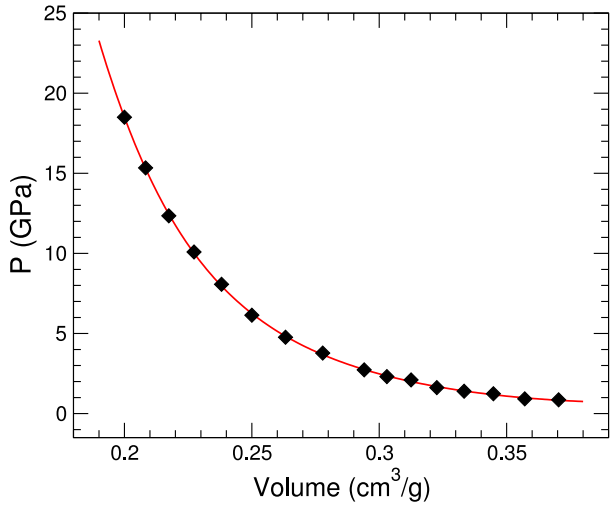

FIG. 3. Pressure evolution with volume along the $T_0 = 4000$ K isotherm. Data points (diamonds) are the MD calculated pressures. The solid (red) line is a fifth polynomial fit using the coefficients γ_n (Table I).

A functional representation of ΔF is now necessary to compute ΔS_T which requires in turn a functional representation of $P(T_0,V)$. The latter is determined from the calculated pressures along a reference isotherm at $T = T_0$. A fifth order fit $P(T_0,V) = \sum_{n=0}^{5} \gamma_n \rho^n$ (with $\rho = 1/V$) is performed on the simulated thermodynamic data points along the isotherm $T_0 = 4000$ K, and the corresponding coefficients γ_n are given in Table I. Results of the fit are plotted in Figure 3, together with the simulated data points.

Having in hand a functional representation of ΔF and ΔE, one can finally write a model function of ΔS_T as

$$\Delta S_T = \frac{1}{T_0}\left[E(T_0,V) - E(T_0,V_0) + \int_{V_0}^{V} P(T,V')dV'\right]. \tag{10}$$

The other entropic contribution, $\Delta S_V = S(T,V) - S(T_0,V)$, used in Eq. (5) can be calculated from a temperature change between T_0 and T at fixed volume V. Thus, an isochoric integration of

$$dS = \frac{dE}{T} = \frac{1}{T}\left(\frac{\partial E}{\partial T}\right)_V dT \tag{11}$$

gives an expression of ΔS_V,

$$\Delta S_V = \int_{T_0}^{T} \frac{1}{T'}\left(\frac{\partial E}{\partial T'}\right)_V dT', \tag{12}$$

where the partial derivative appearing in Eq. (11) is realized from Equation (3).

From these different entropy contributions, Equation (5) can be computed for several thermodynamic conditions in volume and temperature, and using the free energy $F(T,V)$ allows determining the equation of state of liquid germania from Equation (4). Results are plotted in Figure 4 as solid lines while the symbols represent the numerical data from the MD simulations for each isochore. Obviously, we have an excellent agreement of the fitted equation of state (Eq. (4)) that is able to reproduce the thermodynamic data point obtained directly from the simulation. We note that the entire volume 0.2 cm^3/g $< V <$ 0.37 cm^3/g and temperature (1500 K $< T <$ 6000 K) range can be reproduced with confidence.

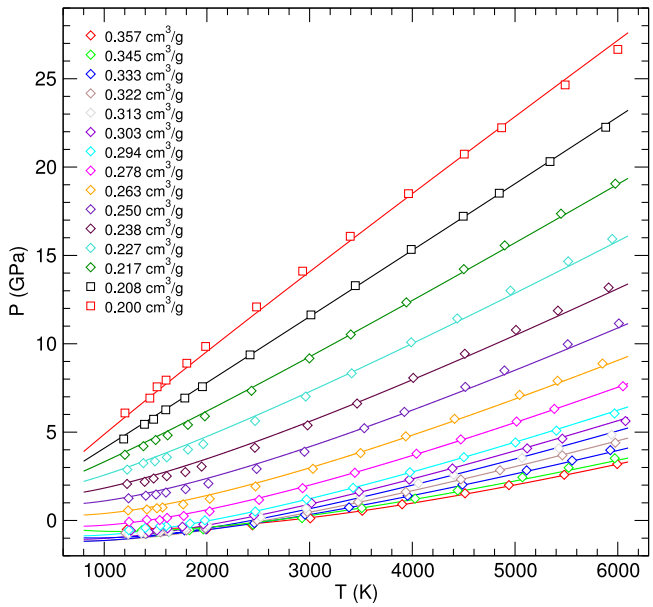

FIG. 4. Pressure evolution with temperature along different isochores. Symbols represent the thermodynamic data points directly calculated from MD, whereas solid lines are the isochoric equations of state using Equation (4).

C. Thermodynamic precursors

Different thermodynamic conditions can now be determined from the parametrized equation of state $P(T,V)$. In the context of LLTs, three curves acting as thermodynamic "*precursors*" are of importance,[20] and we follow here again the strategy developed for water[23] and silica[37] to detect a possible LLT.

A first condition is related to the TMD. It expresses the temperature at which the pressure is minimal for a given volume, and such TMD lines have been found not only in water[44] and silica[45] but also in another tetrahedral liquid (BeF_2[46]). The condition of temperature of maximum density is given by the following expression:

$$\left(\frac{\partial P}{\partial T}\right)_V = 0. \tag{13}$$

The presence of a TMD line is found to be correlated to the transformation of tetrahedral to octahedral order, and also to local structural order parameters[47] defining orientational and translational order, in relationship with a pair correlation entropy maximum,[46] as discussed below.

The second condition or precursor is the spinodal line which is the usual consequence of a demixing phenomenon between two liquids. Such a line is rather well characterized in the case of demixing of a binary compound, and corresponds to an inflexion point of the free energy F, with the second derivative of F being performed with respect to the compound concentration.[48] In a LLT driven by density/volume changes, one can define a similar inflexion point[37] for the free energy,

$$\left(\frac{\partial^2 F}{\partial V^2}\right)_T = -\left(\frac{\partial P}{\partial V}\right)_T = 0. \tag{14}$$

Finally, a third condition has been proposed by Sciortino and co-workers,[37] corresponding to the "K_T^{max}" (or Widom line) which defines the maximum of the isothermal compressibility K_T with respect to the volume,

$$\left(\frac{\partial K_T}{\partial V}\right)_T = 0, \tag{15}$$

with the isothermal compressibility given by

$$K_T = -\frac{1}{V}\left(\frac{\partial V}{\partial P}\right)_T = 0. \tag{16}$$

An inspection of Fig. 4 immediately reveals that germania does not have a minimum in the $P(T)$ curve which indicates directly that a TMD line cannot be found in the investigated temperature range. However, it can be seen that there is a tendency towards a TMD line at low temperatures and elevated volumes, which is hidden by the slowing down of the dynamics for $T \leq 1200$ K.

These three conditions (13)–(15) are now represented in Fig. 5. It is found that a possible spinodal line builds up at

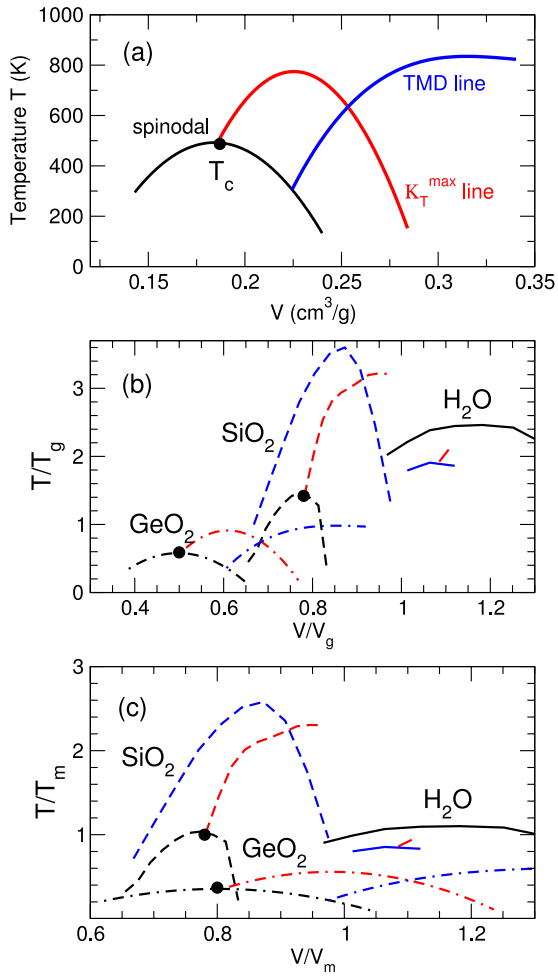

FIG. 5. (a) Results of Equations (13)–(15) defining a TMD line (blue), a spinodal (black), and the maximum of the isothermal compressibility (red) for liquid germania. (b) Comparison of the present results with those of BKS silica[37] and ST2/SPCE water.[28,46,49] Data have been rescaled with respect to their experimental glass transition temperature (850 K, 1450 K and 130 K[50] for GeO_2, SiO_2, and H_2O, respectively), and with respect to the volume of the corresponding glasses (0.37 cm^3/g, 0.45 cm^3/g, and 0.94 cm^3/g, respectively). Note that the water data arise from different MD potentials. (c) Same figure as panel (b) but data have now been rescaled with respect to their experimental melting temperature T_m and volume V_m at zero pressure (1388 K, 2023 K, and 273 K for GeO_2, SiO_2, and H_2O, respectively) and ($V_m = 0.23$ cm^3/g, 0.45 cm^3/g, and 1.00 cm^3/g, respectively).

very low temperatures (typically 200-500 K) and at small volumes (0.15-0.25 cm^3/g) corresponding to densities of about 5.0 g/cm^3. The "K_T^{max}" *line* and the TMD lines are found at somewhat larger volumes and temperatures. A critical point is found at T_c = 483 K and V_c = 0.18(7) cm^3/g.

D. Discussion

It is important to emphasize that all curves lie in a (V,T) domain that is *outside* the investigated range from equilibrated MD simulations which is a serious drawback of the application to GeO_2. There is a simple reason for this. The laboratory glass transition (850 K) and the numerical glass transition regions are larger than those (200-700 K) involved in the three conditions (13)–(15), but they are also smaller than the temperatures of the investigated range of equilibrated data points (1200 K-6000 K). As a consequence, one can neither obtain equilibrated (T,V,P) numerical data points that could serve as input for the fitting procedure using Eq. (2) nor an equilibrium energy $E(T,V)$ in the (T,V) range where the three conditions can eventually be met. One must, therefore, have confidence in the fit performed at higher temperatures and in its extrapolation to lower temperatures. Still, we find that our critical temperature T_c is in reasonable agreement with the one proposed from an experimental phase diagram,[10] suggesting that one has $T_c \simeq 1000$ K and P_c = 4 GPa for liquid germania. Using our fits of Eq. (4) and the determined value of V_c = 0.18(7) cm^3/g (Fig. 5(a)), we arrive to a similar critical pressure (P_c = 3.1 GPa). An additional signature of thermodynamic instability that may lead to a LLT is provided by the behavior of the coefficient $a(V)$ which is equal to the zero temperature value $U(0,V)$ (Helmholtz free energy) or $F(0,V)$. Given that $a(V)$ exhibits a negative curvature with increasing volume (Fig. 2), i.e., it indicates that the condition of stability of a single phase $(\partial^2 F/\partial V^2)_T > 0$ is not satisfied, and suggests that GeO_2 might undergo a phase separation at low temperature and high volume.

Similar features (i.e., a spinodal at $T \leq T_g$) are actually observed in potassium silicates and the corresponding spinodal line is driven by changes in composition. It has been found, indeed, that the consulate point (i.e., the temperature maximum) of the miscibility gap in K_2O–SiO_2 melts is below the glass transition temperature.[38,51,52] Despite this, phase separation which is a consequence of liquid immiscibility has been evidenced.[53,54]

In liquid germania using the same OE potential, Jabes *et al.*[46] find a TMD line in the deep supercooled liquid (1350-1400 K) and over a very narrow range in volume (0.24-0.25 cm^3/g), a situation which substantially contrasts with other tetrahedral systems such as water, silica, or BeF_2 for which the TMD line is found to be quite far away from the glass transition region, e.g., for silica the TMD region extends from 0.33 to 0.5 cm^3/g and 4000-5000 K,[37,46] i.e., at temperatures which are much larger than the numerical glass transition temperature (2000 K).

We then compare the findings with those obtained for a Born-Kramer-Van Santen (BKS) simulated silica (Fig. 5(b)). Even when the behavior in (T,V) of the thermodynamic precursors is rescaled with respect to the measured glass transition temperature T_g and to the (glass) volume at zero pressure and low temperature (V_g), the location of the thermodynamic precursors appears to be quite different. First, the critical point of silica is found in the liquid or supercooled régime at $T > T_g$, and at volumes that are close to V_g, in sharp contrast with the present result on germania. One furthermore notices that the TMD line of germania is found to be located at volumes fulfilling $V > V_c$ only, whereas it displays a maximum value at $V/V_g \simeq 0.85$ in the case of silica. When rescaled with respect to the melting points (T_m and V_m) of the low density crystalline phases (e.g., cristoballite), it is furthermore detected (Fig. 5(c)) that while the location of T_c of both silica and water is rather similar, and close to their corresponding melting temperature, the location of the germania critical point is found to be much lower. However, the volume V_c/V_m appears to be similar for silica and germania. This might suggest that for both systems, similar changes under isochoric transformations could be observed along the isotherm $T = T_c$.

In silica, Sciortino and co-workers[37] characterize independently the existence of a LLT by detecting at the relevant (T,V) condition structural changes in the vicinity of the silicon atom. Specifically, for $T < T_c$, the fifth oxygen neighbor distribution is unimodal and lies outside of the first coordination shell. However, as T approaches T_c, this distribution becomes bimodal which indicates that two distinct populations are present in the liquid. The presence of two coordination environments, thus, provides a possible structural signature of LLT, while also substantiating the analysis from the thermodynamic precursors. Following this path, we have analyzed in a similar fashion the structural correlations in densified liquid GeO_2 along an isotherm ($T_c \simeq 400$ K) from the available volume range. Figure 6 shows the results of the Ge-centred partial pair correlation function $g_{Ge}(r)$ at V = 0.37 cm^3/g. A

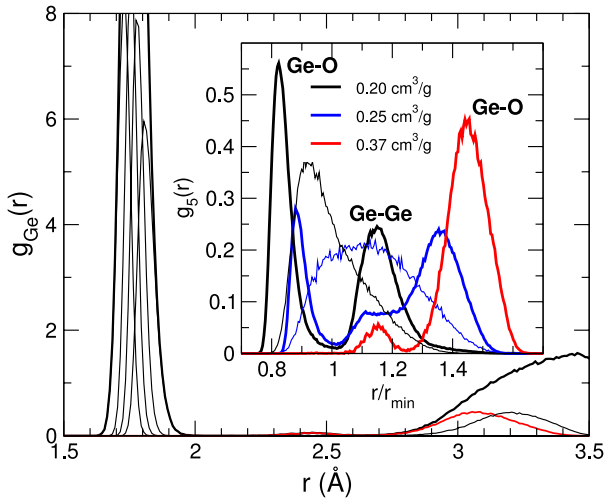

FIG. 6. (a) Decomposition of the partial pair correlation function $g_{Ge}(r)$ of a 400 K germania system into Ge-centred neighbor distributions. Here, V = 0.37 cm^3/g. The red curve represents the fifth neighbor distribution $g_5(r)$. The inset shows the evolution of $g_5(r)$ for selected volumes and temperatures (400 K thick lines and 2500 K thin lines), including in the vicinity of the critical point (Fig. 5(a)). The x-axis has been rescaled with respect to the minimum r_{min} of $g_{GeO}(r)$ which permits splitting the first and the second shells of neighbors. One has r_{min} = 2.12 Å, 2.19 Å, and 2.24 Å for 0.37, 0.40, and 0.50 cm^3/g, respectively. Contributions due to Ge–O and Ge–Ge correlations are indicated (see text for details).

decomposition into neighbor distributions shows that only four neighbors are part of the first coordination shell, as expected[9,12] for low temperature germania at ambient conditions (V_g), and these all correspond to the Ge–O correlations of the tetrahedra. The fifth neighbor distribution $g_5(r)$ (red curve in Fig. 6) belongs to the second shell of neighbors ($r > r_{min}$ and $r/r_{min} = 1.45$) and corresponding oxygen atoms are associated with the second ($r/r_{min} \simeq 1.45$) neighbouring $GeO_{4/2}$ tetrahedra at a distance of 3.07 Å.[9] We furthermore note a minuscule contribution from Ge–Ge correlations ($r/r_{min} = 1.15$). However, as the volume decreases to values corresponding to the *loci* of the thermodynamic precursors, similarly to silica, the distribution of $g_5(r)$ becomes bimodal within and without the first coordination shell, and signals that the fifth neighbor has now two well-defined possibilities and is found to be species related. In fact, a decomposition of $g_{Ge}(r)$ into correlations arising from Ge and O atoms shows that the fifth neighbor in the first coordination shell ($r/r_{min} < 1$) is entirely due to Ge–O correlations for $V = 0.25$ cm^3/g, whereas a shoulder peak builds up at $r/r_{min} = 1.15$ that arises only from Ge–Ge correlations. However, this distance is somewhat smaller than the Ge–Ge correlating distance that comes from Ge–O–Ge linkages. An inspection of the corresponding structure shows that this shoulder peak originates from the growing presence of edge-sharing (ES) tetrahedra/polyhedra, similarly to chalcogenides[55] that lead to a typical distance of 2.50-2.55 Å, i.e., $r/r_{min} \simeq 1.15$. This tendency is enhanced as the critical point is approached ($V = 0.20$ cm^3/g). On the other hand, the behavior of the very first neighbor distributions (from $g_1(r)$ to $g_4(r)$) do not change much under volume change, and the fifth neighbour distribution outside the first shell of neighbours comes from the Ge–Ge correlations of ES connections. Given that these findings bear obvious similarities with the silica liquid,[37] it provides some support to the possibility of a LLT in the determined thermodynamic (T,V) domain for germania, although the detail of the Si or O contributions to $g_5(r)$ has not been reported. The same analysis on a high temperature liquid satisfying $T > T_c$ (2500 K, inset of Fig. 6) shows that these features have completely vanished, and instead a broad distribution over distances $0.8 < r/r_{min} < 1.5$ is found. These dramatic changes also indicate the important structural modifications with temperatures decrease, and once the liquid has densified.

IV. DYNAMICS, STRUCTURE, AND TOPOLOGICAL CONSTRAINTS

A. Dynamics

We now investigate the effect of volume change on the dynamics.

1. Diffusivity

An appropriate means to probe the dynamics is to compute the mean-square displacement of an atom of type α in the melt, given by

$$\langle r^2(t)\rangle = \frac{1}{N_\alpha}\sum_{i=1}^{N_\alpha}\langle|\mathbf{r}_i(t) - \mathbf{r}_i(0)|^2\rangle, \qquad (17)$$

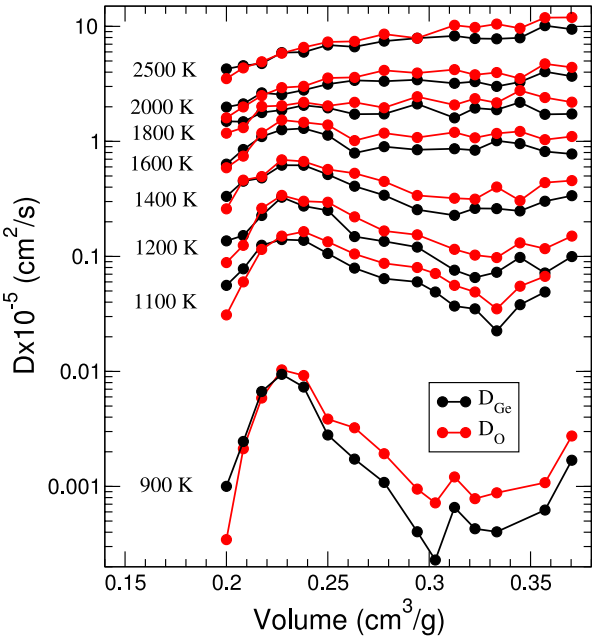

FIG. 7. Isothermal diffusivities for germanium (red) and oxygen (black) in liquid germania as a function of volume system.

where N_α is the number of atoms of species α. The dependence of $\langle r^2(t)\rangle$ at long times becomes linear and signals the onset of diffusion. Using the Einstein relation $\lim_{t\to\infty}\langle r^2(t)\rangle/6t = D$, one can have access to the diffusion constants D for both oxygen and germanium atoms at selected isotherms, and these are represented in Fig. 7.

Fig. 7 shows a clear diffusivity maximum D_{max} at $V \simeq 0.23$ cm^3/g, and a diffusivity minimum D_{min} at $V \simeq 0.32$ cm^3/g for both Ge and O atoms, and these extrema tend to become more marked as the temperature is decreased (e.g., 900 K). Here, we recover previous diffusivity results obtained for liquid germania using the same potential,[46] and extrema were also found for isotherms found between 1300 K $\leq T \leq$ 1600 K. However, our results span over larger volume and temperature variations, allowing for an extended investigation in an Arrhenius representation (Fig. 8(a)).

Self-diffusion constants are plotted for the system of interest as a function of the inverse temperature, revealing an Arrhenius behavior (Fig. 8(a)). This behavior of the form $D = D_0 \exp[-E_A/k_BT]$ is found to be rather well satisfied for the equilibrated liquids, but a progressive deviation (curvature) sets in for lower temperatures (900 K, i.e., $10^3T = 1.11$). For the high temperature régime, it can be remarked that the corresponding slope (i.e., the activation energy E_A for diffusion) depends on the volume V of the system, as noticed from the different slopes for $D(1/T)$ at fixed volume. When E_A is followed as a function of V (Fig. 8(b)), one furthermore remarks that E_A goes through a minimum for volumes fixed between roughly 0.22 cm^3/g and 0.26 cm^3/g. When compared to Fig. 7 representing D as a function of V along a selected isotherm, one realizes that the region where one has D_{max} coincides with an activation energy minimum for diffusivities. This correlation signals that when energy barriers for viscous flow are low, transport properties are optimized and lead to an enhanced diffusion that results in a D_{max}.

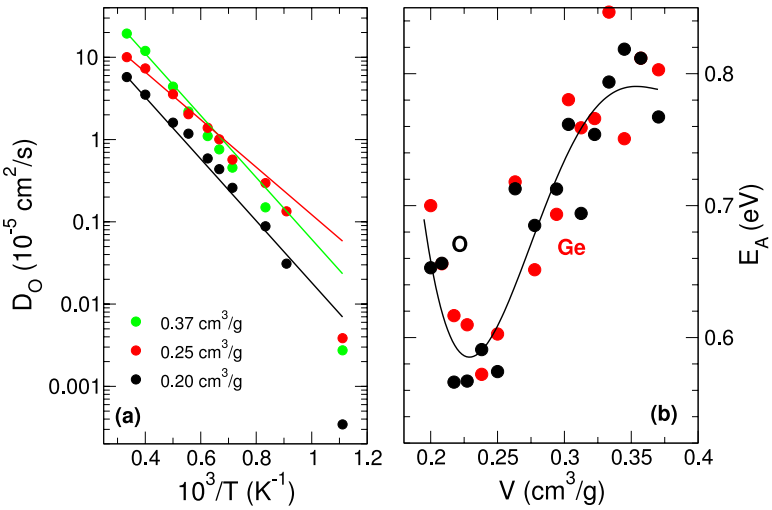

FIG. 8. (a) Arrhenius plot of oxygen diffusivity for selected system volumes. (b) Activation energy for germanium (red) and oxygen diffusion (black) as a function of system volume. The solid line is a quadratic fit to the global set of data.

In addition, assuming that the glass transition temperature T_g does not evolve much with volume, and using the known formula[56] $\mathcal{M}(V) = \mathrm{E}_A \ln_{10} 2/k_B \mathrm{T}_g(V)$, one can conjecture that the minimum in $E_A(V)$ (Fig. 8(b)) might induce a minimum in liquid fragility for $V \simeq 0.23$ cm^3/g. Such a conjecture is supported from similar results on another densified tetrahedral system, namely, $2SiO_2$–Na_2O.[57] For the latter, the location of D_{max} was found to correlate with the minimum in activation energy E_A for both viscosity and diffusivity, and also with a minimum in viscosity.

2. Relaxation behavior

Since an anomalous behavior is obtained for the activation energy E_A, and for D, one may wonder if this results from a particular relaxation behavior.

Additional information can therefore be gathered from the density correlations which provide an interesting means to decode the obtained anomalies in dynamics. We have computed the intermediate scattering function $F_s(k,t)$ for a given isotherm (1400 K) exhibiting well defined diffusivity anomalies at D_{max} and D_{min}. This function follows the Fourier components of density correlations and characterizes the slowing down of the relaxation as one approaches the glass transition. We focus in the forthcoming on this function at the wavevector $k = k_{max}$, the principal peak position of the static structure factor $S(k)$.

Figure 9(a) represents $F_s(k,t)$ for all investigated system volumes. $F_s(k,t)$ exhibits the usual two step relaxation behavior with a small β-relaxation[58] plateau behavior (e.g., at $F_s(k,t) \simeq 0.40$ for $V = 0.37$ cm^3/g) that is similar to the case of silica.[59] When investigated along the present isotherm (1400 K) as a function of volume, it is seen that the $F_s(k,t)$ shifts to higher times, thus indicating that the system needs more time to relax to equilibrium ($F_s(k,t) = 0$), the lowest volume (0.20 cm^3/g) exhibiting the slowest dynamics, and a β-relaxation plateau that is found to be substantially higher. A standard means[60] of evaluating a relaxation time τ is to calculate the time at which one has $F_s(k,t) = 1/\mathrm{e}$, and corresponding results are represented in Fig. 9(b). It is found that the diffusivity maximum D_{max} coincides with a local minimum in relaxation time $\tau(V)$ at $V \simeq 0.25$ cm^3/g that permits to relax to equilibrium on time scales that are of about 2 ps. Finally, we note that the smallest relaxation time is found for the liquid at nearly ambient pressure and volume $V_g = 0.37$ cm^3/g corresponding to the glass density.

B. Pair correlation entropies and diffusivity scaling

The diffusivity results represented in Fig. 7 actually recover an interesting relationship between diffusion and the pair correlation entropy defined by

$$S_2/k_B N = -\frac{2\pi}{V} \sum_{i,j} x_i x_j \int_0^\infty \Big[g_{ij}(r) \ln g_{ij}(r) - [g_{ij}(r) - 1] \Big] r^2 dr, \quad (18)$$

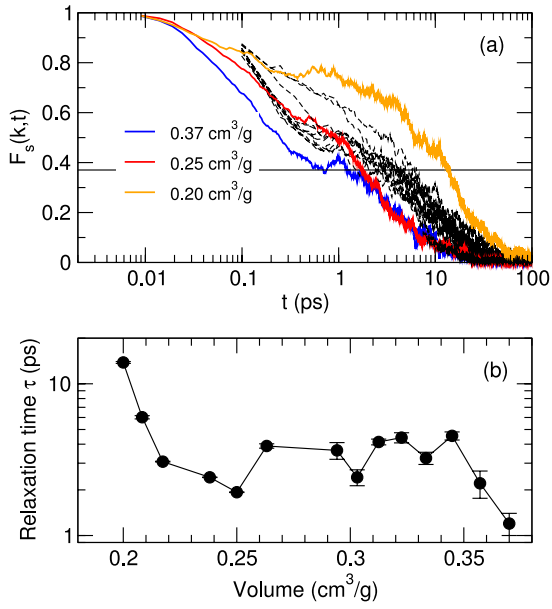

FIG. 9. (a) Oxygen intermediate scattering function for different volumes at $T = 1400$ K at $k = k_{max} = 2.4$ Å^{-1}. The thin lines correspond to all volumes different from 0.37, 0.25, and 0.20 cm^3/g. The horizontal line corresponds to 1/e. (b) Calculated relaxation time τ as a function of system volume V for 1400 K.

where g_{ij} are the partial pair correlation functions, and x_i and x_j represent the molecular fraction of species i and j (Ge,O). This entropy is defined[31,61] as the difference between the entropy of a liquid and the one of an ideal gas[62] at the same temperature and density and can be accessed from numerical simulations[63] by expanding correlation functions. Here, it has been shown that while S_2 represents a reasonable estimate of the excess entropy of the liquid, it connects to transport, structure, thermodynamics, and mobility in liquids, as also recently emphasized from the investigation of a set of densified tetrahedral liquids[46] among which, GeO_2. We also find that for the isotherms exhibiting the most pronounced extrema in diffusivity (1200 K and 1400 K, Fig. 7), the calculated entropy using Eq. (18) displays the same trend as D (Fig. 10(a)), i.e., a clear maximum in S_2 is found at around 0.22 cm^3/g, whereas a broad minimum is obtained for the 1400 K isotherm, centred at $V \simeq 0.32$ cm^3/g. The calculated values of S_2 are actually very close to those found[46] in a previous study of GeO_2.

The connection with transport can be quantified by rescaling the diffusivity D via

$$D^* = \frac{D}{V^{1/3}\sqrt{\frac{k_B T}{m}}}. \tag{19}$$

Rosenfeld and others[35,64] have shown that diffusivity, viscosity, and thermal conductivity in simple liquids follow a simple semiempirical relationship of the form $A \exp \alpha S_e$ and is satisfied for a variety of complex liquids.[65–68] Here, S_e stands for the excess entropy of the liquid with respect to the corresponding ideal gas, and in dense liquids it is essentially driven by the effect of the interactions that lead to structural correlations (i.e., the functions g_{ij}). As a result, a convenient way[31–34,46,68] to check for such scaling laws is to compare the calculated diffusivities with the pair correlation entropy S_2. Fig. 10(b) shows the dimensionless diffusivity results using Eq. (19) as a function of the pair correlation entropy (Eq. (18)). It is seen that the correlation is very well satisfied for the three considered isotherms, and a global fit for the whole data leads to $\alpha = 1.41$. One has furthermore $\alpha = 2.41$, 1.49, and 1.13 for the separate isotherms 1100 K, 1200 K, and 1400 K, respectively. For the same range of temperatures ($T > 1200$ K), these values are slightly lower than those determined from isochoric fits (1.67-1.73) extracted from a set of numerical data on densified germania[46] but the result is expected and has been pointed out from a separate Rosenfeld-type fit on isochores and numerical isotherm of diffusivity/entropy data of liquid silicon.[69]

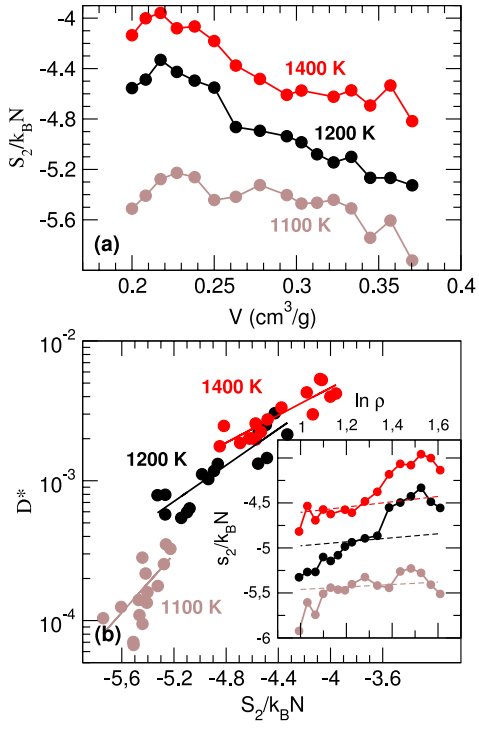

FIG. 10. (a) Pair correlation entropy S_2 as a function of volume in liquid germania for three selected isotherms (1100 K, 1200 K, and 1400 K). (b) Rosenfeld scaled diffusivity D^* as a function of pair correlation entropy S_2. The solid lines are fits using $A \exp \alpha S_2$ for a given isotherm. The inset shows the behavior of S_2 with ln ρ and serves for the discussion on anomalous diffusivity criteria[31] (see text for details). Broken lines have a slope of $1/3\alpha$ and serve for comparison.

Although the Rosenfeld-type scaling law is found to agree for the present germania liquid, it is possible to test an additional probe for the presence of entropy driven diffusivity extrema as proposed in Refs. 31 and 69. Assuming that a Rosenfeld-type scaling holds, one can take the partial derivative of Eq. (19) with the scaling form, and one obtains

$$\left(\frac{\partial S_e}{\partial \ln \rho}\right)_T = \frac{1}{3\alpha}\left[1 + 3\left(\frac{\partial \ln D}{\partial \ln \rho}\right)_T\right] \tag{20}$$

and in this case a criterion[31] for the observation of an anomalous diffusivity will be given by

$$\left(\frac{\partial S_e}{\partial \ln \rho}\right)_T > \frac{1}{3|\alpha|}, \tag{21}$$

where we remind that α appears in the functional representation of the rescaled diffusivities $D^* = A \exp[\alpha S_e]$. From the inset of Fig. 10(b), it is seen that when the excess entropy is represented as a function of ln ρ and when the slopes of $S_2(\ln(\rho))$ are compared to the value of $1/3|\alpha|$, condition (21) holds more or less for the regions in thermodynamic phase diagram (e.g., $\ln \rho < 1.2$, $\ln \rho > 1.3$ for $T = 1200$ K) where such diffusivity extrema are obtained. For the different isotherms, one notes, indeed, that the volume range for which the diffusivity maxima are obtained (0.20 $cm^3/g \le V \le 0.25$ cm^3/g), condition (21) is satisfied. In fact, as just described, separate fits along the isotherms using the Rosenfeld scaling (Fig. 10(b)) lead to different parameters α, and when corresponding lines with a slope of $1/3|\alpha_i|$ are represented in a $(\ln \rho, S_2)$ plot (broken lines in the inset), the slope of the excess entropy with ln ρ will always be higher in the region where D_{max} is obtained.

C. Coordination numbers

In real space, we examine the behavior of the coordination number n_{GeO} in liquid germania. Here, we have defined n_{GeO} as the average number of nearest oxygen neighbors in the first coordination shell of a Ge atom,

$$n_{GeO} = \frac{4\pi}{V}\int_0^{r_{min}} r^2 g_{GeO}(r) dr, \tag{22}$$

i.e., we obtain n_{GeO} by integrating up to the corresponding first minima r_{min} the partial pair correlation function $g_{GeO}(r)$

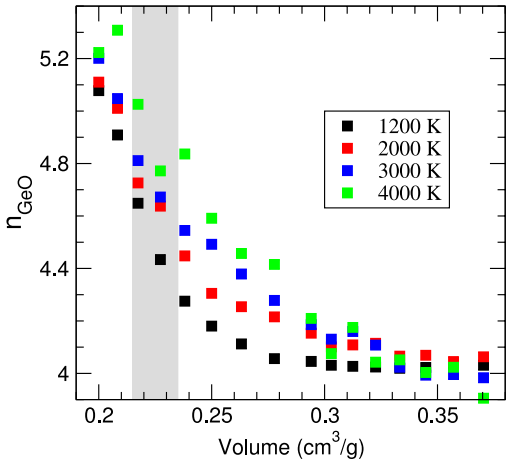

FIG. 11. Behavior of the coordination number n_{GeO} as a function of system volume for different isotherms. The gray zone indicates the volume range where diffusivity anomalies are obtained (see Fig. 7).

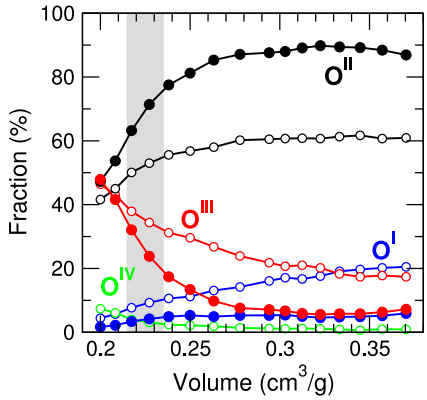

FIG. 13. Behavior of the oxygen coordinated species as a function of system volume V at 1200 K (filled symbols) and 3000 K (open symbols). The gray zone indicates the region of D_{max}.

at the different volumes and temperatures (e.g., Fig. 6). Given the well-defined first minimum of $g_{GeO}(r)$, one has a well-separated shell of nearest-neighbors for a large range of temperatures and volumes. Fig. 11 shows the behavior of n_{GeO} as a function of volume for selected isotherms. It can be seen that the coordination number steadily increases as the volume decreases, this trend being obtained for all temperatures in the range 1200 K $\leq T \leq$ 4000 K. Starting from the "tetrahedral" value $n_{GeO} = 4$, one reaches a coordination number of 5.1-5.3 at $V = 0.2$ cm^3/g, but neither threshold nor anomaly is obtained for volumes at which a diffusivity maximum or minimum is obtained (Fig. 7).

The population of r-coordinated oxygen and germanium species can also be followed, and corresponding results are shown in Figs. 12 and 13 for germanium and oxygen, respectively. At low temperature, the majority of Ge atoms are found to be in tetrahedral environment at the largest volumes (0.37 cm^3/g). However, as the volume is reduced (or pressure increased), higher coordinated species appear. While these manifest, on average, by an increase of n_{GeO} (Fig. 11), the detail of the Ge population shows that five- (Ge^{V}) and six-fold coordinated (Ge^{VI}) Ge atoms are likely to occur, the former being systematically larger (by a factor two) when compared to Ge^{VI}, and already present in the range 0.25 cm^3/g $\leq V \leq$ 0.30 cm^3/g. The presence of this "*intermediate*" coordination is consistent with experiments performed in the glassy state[70] where five-fold Ge atoms have been detected in densified germania, and the fraction of the Ge^{V} species shows an increase from 0% to ≃20% when the volume is reduced from $V = 0.27$ cm^3/g (i.e., $\rho_g = 3.7$ g/cm^3) to 0.20 cm^3/g.

The increase of temperature leads to a lowering of the fraction of Ge^{IV} at large volumes, and also leads to the presence of under-coordinated Ge atoms (Ge^{III}), a feature that is typical of stretched melts[71] having a negative pressure (Fig. 4) which usually contains elements having a coordination number that is lower than the one anticipated by the octet rule. One

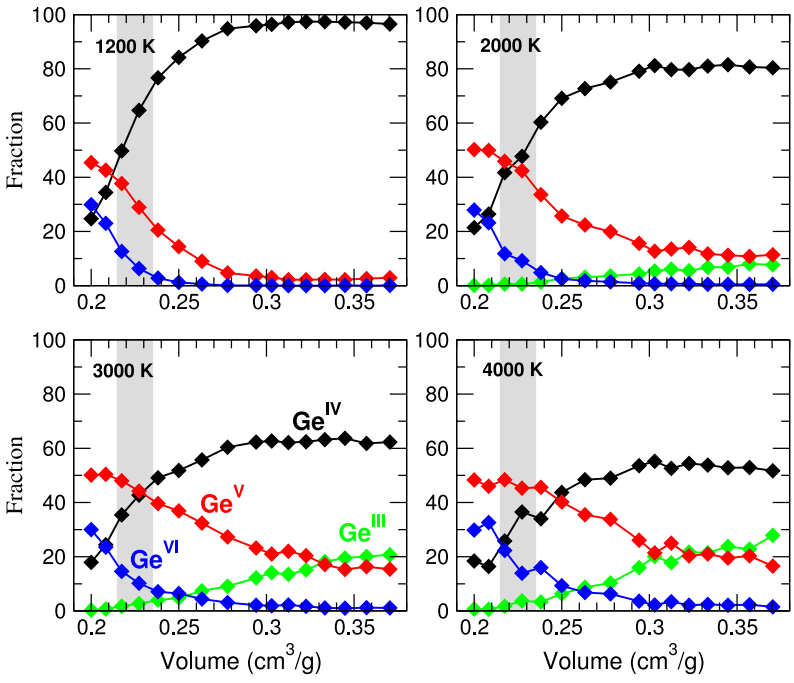

FIG. 12. Behavior of the germanium coordinated species (Ge^{III}, Ge^{IV}, Ge^{V}, and Ge^{VI}) as a function of system volume V at different temperatures. The gray zone indicates the region of D_{max}.

furthermore notes that the fraction of octahedral Ge is nearly temperature independent, and most of the structural changes at short range order are triggered by the five-fold Ge which increases more importantly in the volume range 0.27 $cm^3/g \leq V \leq 0.33\,cm^3/g$. Finally, we remark that the thermodynamic region where the diffusivity maximum is observed, liquids have a no dominant local structure (tetrahedral or octahedral) because all species are found to have a population of the same order (30%-40%), this observation being valid for all considered temperatures.

Similarly, we find that the oxygen speciation behaves quite similarly. Figure 13 displays the fraction of r-fold oxygen species (r = 1,2,3,4) as a function of system volume for two selected temperatures (1200 K and 3000 K), and, again, it is to be noticed that higher coordinated species (O^{III} and to a lesser extent, O^{IV}) populate the liquid network structure as the volume is lowered.

D. Topological constraints

The topology of the liquid structure can be also characterized in the context of coordination number increase and diffusivity anomalies by making a connection with network rigidity, as discussed now. Diffusivity anomalies have been recently detected in liquid sodium silicates[57,72] and have been linked with anomalies in topological constraints, derived from rigidity theory.[73] We follow here the same path. In rigidity theory, the number of dominant interactions which are usually near-neighbor BS and next-near-neighbor BB forces, and the associated number of topological rigid constraints can be exactly computed in a mean-field way,[74–76] and is given by

$$n_c = \frac{\sum\limits_{r\geq 2} n_r[\frac{r}{2} + 2r - 3]}{\sum\limits_{r\geq 2} n_r}, \tag{23}$$

where n_r is the concentration of species being r-fold coordinated. The condition $n_c = 3$ corresponds to the well-known Maxwell stability criterion for isostatic trusses or macroscopic structures.[77] Its application to network glasses has led to the identification of a flexible to rigid transition.[75,76] In contrast with usual applications (e.g., network glass or glass-forming liquids) for which n_c is tuned with composition, here n_c is driven by pressure, as in densified sodium silicates.[57] The two contributions appearing in Eq. (23) arise from (i) BS given that each bond is shared by two neighbors, and one has $r/2$ BS bond-stretching constraints for an r-fold atom, and (ii) BB (angular) constraints. For the latter, one notices that a 2-fold atom involves only one angle, and each additional bond will need the definition of two more angles,[75] leading to the estimate of ($2r$-3).

1. MD based constraints

Equation (23) applies at zero pressure and temperature for fully connected networks. In order to explore an application of topological constraint counting with volume and temperature, and especially for the present thermodynamic domain of interest, one relies on a MD-based enumeration, as introduced recently.[57,78,79] We determine, indeed, topological

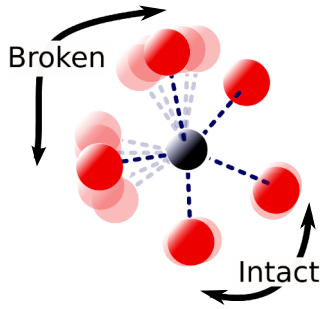

FIG. 14. Schematic method of constraint counting from MD-generated configurations. Large (small) angular excursions around a mean value are characterized by large (small) standard deviations on angular distributions, representing broken (intact) topological constraints.

constraints by following doublets (pairs, bonds) or triplets (angles) of neighbors over the simulated trajectory at a given (T,V,P) condition. One extracts from the radial (angular) motion of such doublets (triplets) a pair (angular) distribution which is characterized by a first moment (i.e., a mean) and a second moment (i.e., a standard deviation) σ_i with $i = r$ or $i = \theta$ depending on the considered situation, bonds, or angles. It quantifies the excursion around the mean value and provides information about the strength of the underlying BS (BB) interaction. If the angular excursion is small, one will identify a corresponding topological constraint (e.g., angular, see Fig. 14), otherwise the constraint is considered as broken and does not contribute to rigidity. We focus in the forthcoming on BB constraints, given that the fraction of Ge and O BS constraints is directly given by $n_{GeO}/2 = n_{Ge}/2$ and by $n_O/2$.

Equation (23) can be made more general by taking into account an explicit (T,V) dependence that is written[80] as

$$n_c(T,V) = \frac{\sum\limits_{i,r} n_r^i(T,V)[\frac{r(T,V)}{2} + q_r^i(T,V)(2r-3)]}{\sum\limits_{i,r} n_r^i(T,V)}, \tag{24}$$

where $q_r^i(T,V)$ is a function quantifying the fraction of broken BB constraints of an r-folded (i = Ge,O) atom, and $n_r(T,V)$ represents the population of r-folded species (Figs. 12 and 13). This function $q_r^i(T,V)$ has two obvious limits because all relevant constraints can be either intact at low temperature (degrees of freedom are all frozen) or entirely broken at high temperature. At a finite temperature however, a fraction of these constraints are broken by thermal activation. Different forms can be proposed for $q_r^i(T,V)$, based either on an energy landscape approach[81] or involving a simple activation energy for broken constraints.[82] A simple step-like function allows obtaining analytical expressions for fragility and glass transition temperature,[80] heat capacity,[83] and hardness[84] as a function of composition for binary and multicomponent glasses.

Figures 15 and 16 now represent the calculated functions $q^{Ge}(T,V)$ and $q^O(T,V)$, respectively, the average over the r-speciation having been performed. At fixed volume, both functions behave as they should, i.e., with increasing temperature and the lowering of the energy barriers associated with BB constraints, one obtains a global decrease of $q^{Ge}(T,V)$ and $q^O(T,V)$, and, at high temperature (2800 K), they are nearly equal to zero, i.e., angles do not contribute to the rigidity of the liquid.

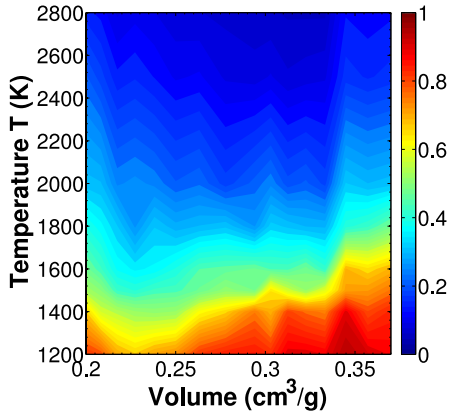

FIG. 15. Contourplot of the fraction $q^{\mathrm{Ge}}(T,V)$ of intact Ge BB constraints.

Several other conclusions emerge from an inspection of the contourplots, especially when they are compared to the obtained anomalies in transport properties (Figs. 7 and 8). It is seen, indeed, that both Ge and O display a minimum in their fraction of BB constraints in the volume range (0.2-0.25 cm^3/g), i.e., roughly in the region where D_{max} is detected. For instance, for $T = 1200$ K $q^{\mathrm{Ge}}(T,V)$ decreases from a value of about 0.82 at $V = 0.2$ cm^3/g to 0.63 for $V = 0.22$ cm^3/g, before increasing again at larger volumes, and to nearly $q^{\mathrm{Ge}}(T,V) = 1$ at $V = 0.35$ cm^3/g. In addition, we note that the existence of a minimum in $q^{\mathrm{Ge}}(T,V)$ can be unambiguously detected as long as $T \leq 1800$ K, i.e., for the temperature range at which a D_{max} can be obtained (Fig. 7). For larger temperatures, $q^{\mathrm{Ge}}(T,V)$ does not exhibit a non-monotonic trend anymore, and so does the diffusivity. One has, thus, a strong correlation between BB constraints and D_i (i = Ge,O). A similar trend is obtained for the corresponding function $q^{O}(T,V)$ (Fig. 16). For the latter, a local maximum emerges in $q^{O}(T,V)$ at 0.33-0.35 cm^3/g (i.e., BB constraints are restored with increasing volume), and this local maximum is found to coincide with the observed D_{min} that is detected for $T \leq 1400$ K only (Fig. 7).

Finally, using Eq. (24), one can evaluate the total density of constraints $n_c(T,V)$, represented in Fig. 17. It can be remarked that the obtained minimum in $q^{\mathrm{Ge}}(T,V)$ and $q^{O}(T,V)$ at 0.2-0.24 cm^3/g induces also a minimum in $n_c(T,V)$ for $T \leq 1800$ K. Interestingly, the deep supercooled liquid (1200 K) is found to be isostatically rigid ($n_c \simeq 3$) for volumes that are

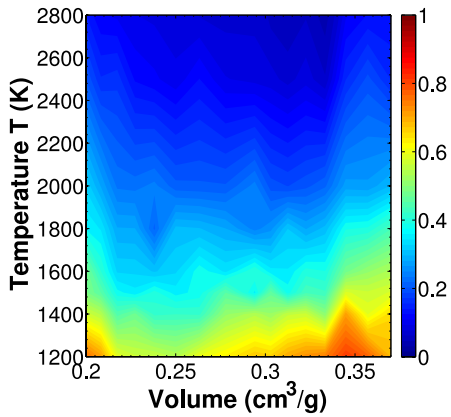

FIG. 16. Contourplot of the fraction $q^{O}(T,V)$ of intact oxygen BB constraints.

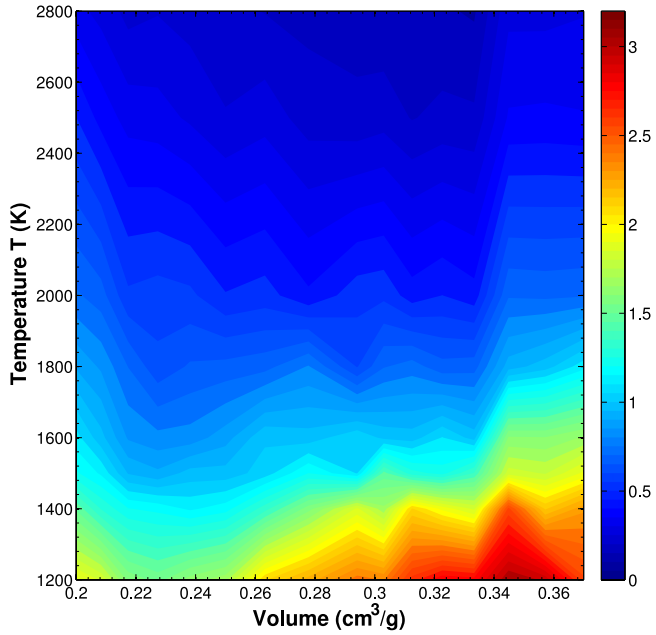

FIG. 17. Contourplot of the total fraction $n_c(T,V)$ of topological constraints.

somewhat lower than the (glass) volume $V_g = 0.37$ cm^3/g. For such systems, a local maximum is detected in $n_c(T,V)$ which is driven by the stiffening of the oxygen BB interactions (i.e., a maximum in $q^{O}(T,V)$, Fig. 16). This signals that germania at ambient pressure is flexible, and becomes isostatically rigid under the effect of a moderate pressure increase, a conclusion that is consistent with reported pressure driven transformations[85] showing that isostatic rigidity (i.e., $n_c = 3$) is achieved in GeO_2 at P $\simeq$ 0.5 GPa. This usually is manifested by space-filling tendencies under annealing and are correlated with the vanishing of low-frequency modes and the distortion of the basic tetrahedra under pressure.[86,87]

2. Adaptive liquids

The physical picture that emerges from the topological analysis is the following. The obtained anomalies (Figs. 15-17) result from the growth of liquid connectivity with volume decrease, which is induced by the tetrahedral to octahedral coordination change (Fig. 12). The increase in connectivity leads in fact to additional stress[74–76] induced by an increase of the number BS constraints which is found to increase with decreasing volume. To counterbalance such effects and accommodate stress, bond-angles increase their angular excursion which leads to a partial softening of the BB interaction and reduces the number of corresponding constraints. At ambient pressure (for $V = V_g$) and low temperature, liquid germania is flexible ($n_c = 2.62$ at 1200 K, Fig. 17).

At the network level, the global increase of BS constraints arising from the growth of r_{Ge} and r_O can be reduced by breaking the energetically softer BB constraints so that $q^{\mathrm{Ge}}(T,V)$ and $q^{O}(T,V)$ tend to decrease at larger volumes. This is network adaptation in a fashion that is very similar to what has been found in rigidity tuned by composition[76,88–90] at ambient pressure. In fact, the observed features display striking similarities with the self-organized intermediate phase found in network

glasses[91–93] where the growing stress induced by cross-linking atoms is partially released over a finite compositional interval fulfilling nearly $n_c \simeq 3$.[94] Similarly, in the present densified germania liquid as both r_{Ge} and r_O continue to increase with decreasing volume, the adaptive behavior can only hold up to a certain point ($\simeq$0.22 cm^3/g). Beyond, the softening of BB constraints can no longer accommodate the steadily increasing pressure-induced stress resulting in an onset of stiffness under pressure,[57] which is manifested by an increase of $q^{Ge}(T,V)$ for smaller volumes.

V. SUMMARY AND CONCLUSION

In this article, we have investigated by MD simulations structural, thermodynamic, dynamic, and topological properties of densified germania, a densified tetrahedral liquid that bears not only similarities but also differences with archetypal systems such as silica or water. In a first part, a thermodynamic framework has been used to determine the equation of state of liquid GeO_2. It is based on the fitting of the system energy which allows to compute an analytical equation of state reproducing very well the simulation data, in line with a previous similar application on SiO_2.[23]

Then, different thermodynamic properties and thermodynamic precursors for a possible detection of LLTs have been derived from the determined equation of state, such as the TMD, the spinodal line, and the maximum of the isothermal compressibility. In the case of germania, such precursors are found at temperatures well below the glass transition temperature, so that their possible signature is hidden by the slowing down of the dynamics. We are aware of only another system (potassium silicates) displaying part (i.e., immiscibility) of these unexpected features. The study of the structure (coordination numbers) shows a steady increase of, e.g., n_{GeO} with decreasing volume, and in the region of the spinodal line no marked change is obtained.

In a second part, we have detected diffusivity anomalies, which manifest for a given isotherm by a maximum and a minimum with volume in the germanium and oxygen diffusion constant. In addition, it has been found that the diffusivity maximum is correlated with a minimum in activation energy which signals the possibility to have strong glass-forming liquids with a lower fragility index. We have then established a relationship between such diffusivity anomalies and topological constraints characterizing the liquid rigidity. It has been found that the diffusivity anomaly D_{max} takes place in a thermodynamic region (T,V) where angles soften and experience larger bond angle excursions in order to accommodate the stress induced by the increase of the oxygen and germanium coordination numbers which induce an increase of the number of bond-stretching interactions. This provides evidence that such an angular adaptation drives the observed anomalies in diffusivities by reducing the liquid rigidity.

To which extent this result has a general ground and may be also valid for other tetrahedral systems is a question of great interest but open at this stage. However, evidence for its general character is supported by the recent example of densified silicates[57,72,94] showing exactly the same salient features and relationship between transport anomalies and isostatic rigidity.

ACKNOWLEDGMENTS

M.M. acknowledges support from the Franco-American Fulbright Commission and International Materials Institute (H. Jain). Mathieu Bauchy and Dan Skoncz-Traintz are gratefully acknowledged for stimulating discussions.

[1]M. Micoulaut, L. Cormier, and G. S. Henderson, J. Phys.: Condens. Matter **18**, R753 (2006).
[2]J. P. Itié, A. Polian, G. Calas, J. Petiau, A. Fontaine, and H. Tolentino, Phys. Rev. Lett. **63**, 398 (1989).
[3]C. Meade, R. J. Hemley, and H. K. Mao, Phys. Rev. Lett. **69**, 1387 (1992).
[4]S. Sugai and A. Onodera, Phys. Rev. Lett. **77**, 4210 (1996).
[5]K. Wezka, P. S. Salmon, A. Zeidler, D. A. Whittaker, J. Drewitt, S. Klotz, H. E. Fischer, and D. Marrocchelli, J. Phys.: Condens. Matter **24**, 502101 (2012).
[6]K. Trachenko and M. T. Dove, Phys. Rev. B **67**, 064107 (2003).
[7]R. D. Oeffner and S. R. Elliott, Phys. Rev. B **58**, 14791 (1998).
[8]E. Yu Tonkov, *High Pressure Phase Transformations. A Handbook* (Gordon and Breach, Philadelphia, 1992).
[9]M. Micoulaut, Y. Guissani, and B. Guillot, Phys. Rev. E **73**, 031504 (2006).
[10]V. V. Brazhkin and A. G. Lyapin, J. Phys.: Condens. Matter **15**, 6059 (2003).
[11]M. Micoulaut, J. Phys.: Condens. Matter **16**, L131 (2004).
[12]D. Marrocchelli, M. Salanne, and P. A. Madden, J. Phys.: Condens. Matter **22**, 152102 (2010).
[13]G. Gutierrez and J. Rogan, Phys. Rev. E **69**, 031201 (2004).
[14]M. Micoulaut, X. Yuan, and L. W. Hobbs, J. Non-Cryst. Solids **353**, 1961 (2007).
[15]V. V. Brazhkin, R. N. Voloshin, A. G. Lyapin, and S. V. Popova, Phys.-Usp. **46**, 1283 (2003).
[16]I. Jackson, Phys. Earth Planet. Inter. **13**, 218 (1976).
[17]O. B. Tsiok, V. V. Brazhkin, A. G. Lyapin, and L. G. Khvostantsev, Phys. Rev. Lett. **80**, 999 (1998).
[18]S. Harrington, R. Zhang, P. H. Poole, F. Sciortino, and H. E. Stanley, Phys. Rev. Lett. **78**, 2409 (1997).
[19]P. H. Poole, F. Sciortino, U. Essmann, and H. E. Stanley, Nature **360**, 324 (1992).
[20]F. Sciortino, P. H. Poole, U. Essmann, and H. E. Stanley, Phys. Rev. E **48**, 727 (1997).
[21]P. H. Poole, F. Sciortino, U. Essmann, and H. E. Stanley, Phys. Rev. E **48**, 4605 (1993).
[22]H. E. Stanley, C. A. Angell, U. Essmann, M. Hemmati, P. H. Poole, and F. Sciortino, Physica A **205**, 122 (1994).
[23]S. R. Elliott, *Physics of Amorphous Materials* (Longman Scientific, London, 1990).
[24]C. A. Angell and H. Kanno, Science **193**, 1121 (1982).
[25]O. Mishima and H. E. Stanley, Nature **396**, 329 (1998).
[26]P. Debenedetti, J. Phys.: Condens. Matter **15**, R1669 (2003).
[27]H. Tanaka, Nature **380**, 328 (1996).
[28]F. Sciortino, P. H. Poole, U. Essmann, and H. E. Stanley, Phys. Rev. E **55**, 727 (1997).
[29]P. H. Poole, F. Sciortino, T. Grande, G. E. Stanley, and C. A. Angell, Phys. Rev. Lett. **73**, 1632 (1994).
[30]T. M. Truskett, P. G. Debenedetti, S. Sastry, and S. Torquato, J. Chem. Phys. **111**, 2647 (1999).
[31]J. R. Errington, T. M. Truskett, and J. Mittal, J. Chem. Phys. **125**, 244502 (2006).
[32]M. Agarwal, M. Singh, B. S. Jabes, and C. Chakravarty, J. Chem. Phys. **134**, 014502 (2011).
[33]B. S. Jabes and C. Chakravarty, J. Chem. Phys. **136**, 144507 (2012).
[34]D. Nayar and C. Chakravarty, Phys. Chem. Chem. Phys. **15**, 14162 (2013).
[35]Y. Rosenfeld, Phys. Rev. A **15**, 2545 (1977).
[36]V. Holten and M. A. Anisimov, Sci. Rep. **2**, 713 (2012).
[37]I. Sakai-Voivod, F. Sciortino, and P. H. Poole, Phys. Rev. E **63**, 011202 (2000).
[38]R. J. Charles, J. Am. Ceram. Soc. **50**, 631 (1967).

[39]R. Rompicharla, D. I. Novita, P. Chen, P. Boolchand, M. Micoulaut, and W. Huff, J. Phys.: Condens. Matter **20**, 202101 (2008).
[40]Y. Guissani and B. Guillot, J. Chem. Phys. **104**, 7633 (1996).
[41]T. Tsuchiya, T. Yamanaka, and M. Matsui, Phys. Chem. Miner. **27**, 149 (2000).
[42]V. Van Hoang, J. Phys.: Condens. Matter **18**, 777 (2006).
[43]Y. Rosenfeld and P. Tarazona, Mol. Phys. **95**, 141 (1998).
[44]J. R. Errington and P. G. Debenedetti, Nature **409**, 318 (2001).
[45]M. S. Shell, P. G. Debenedetti, and A. Z. Panagiotopoulos, Phys. Rev. E **66**, 011202 (2002).
[46]B. S. Jabes, M. Agarwal, and C. Chakravarty, J. Chem. Phys. **132**, 234507 (2010).
[47]P. L. Chau and A. J. Hardwick, Mol. Phys. **93**, 511 (1998).
[48]P. Hudon and D. R. Baker, J. Non-Cryst. Solids **303**, 299 (2002).
[49]P. H. Poole, F. Sciortino, U. Essmann, and H. E. Stanley, Phys. Rev. E **48**, 3799 (1993).
[50]S. Capaccioli and K. L. Ngai, J. Chem. Phys. **135**, 104504 (2011).
[51]J. Schroeder, R. Mohr, P. B. Macedo, and C. J. Montrose, J. Am. Ceram. Soc. **56**, 510 (1973).
[52]J. Schroeder, C. J. Montrose, and P. B. Macedo, J. Chem. Phys. **63**, 2907 (1975).
[53]R. J. Charles, J. Am. Ceram. Soc. **49**, 55 (1966).
[54]Y. P. Gupta and U. D. Mishra, J. Phys. Chem. Solids **30**, 1327 (1969).
[55]C. Massobrio, M. Micoulaut, and P. S. Salmon, Solid State Sci. **12**, 199 (2010).
[56]M. Micoulaut, J. Phys.: Condens. Matter **22**, 285101 (2010).
[57]M. Bauchy and M. Micoulaut, Phys. Rev. Lett. **110**, 095501 (2013).
[58]P. G. Debenedetti and F. H. Stillinger, Nature **410**, 259 (2001).
[59]J. Horbach and W. Kob, Phys. Rev. B **60**, 3169 (1999).
[60]W. Kob and H. C. Andersen, Phys. Rev. E **52**, 4134 (1995).
[61]R. Sharma, M. Agarwal, and S. Chakravarty, Mol. Phys. **106**, 1925 (2006).
[62]R. E. Nettleton and M. S. Green, J. Chem. Phys. **29**, 1365 (1958).
[63]A. Baranayai and D. J. Evans, Phys. Rev. A **40**, 3817 (1989).
[64]M. Dzugutov, Nature **381**, 137 (1996).
[65]J. J. Hoyt, M. Asta, and B. Sadigh, Phys. Rev. Lett. **85**, 594 (2000).
[66]E. H. Abramson, Phys. Rev. E **76**, 051203 (2007).
[67]M. Agarwal and S. Chakravarty, Phys. Rev. E **79**, 030202(R) (2009).
[68]G. Goel, D. J. Lacks, and J. A. Van Orman, Phys. Rev. E **84**, 051506 (2011).
[69]V. V. Vasisht, J. Mathew, S. Sengupta, and S. Sastry, J. Chem. Phys. **141**, 124501 (2014).
[70]G. Lelong, L. Cormier, G. Ferlat, V. Giordano, G. S. Henderson, A. Shukla, and G. Calas, Phys. Rev. B **85**, 134202 (2012).
[71]P. F. MacMillan, Am. Mineral. **69**, 622 (1984).
[72]M. Micoulaut and M. Bauchy, Phys. Status Solidi B **250**, 976 (2013).
[73]*Rigidity Theory and Applications*, edited by M. F. Thorpe and P. M. Duxbury (Kluwer Academic; Plenum Publishers, New York, 1999).
[74]J. C. Phillips, J. Non-Cryst. Solids **34**, 153 (1979).
[75]H. He and M. F. Thorpe, Phys. Rev. Lett. **54**, 2107 (1985).
[76]M. Micoulaut and J. C. Phillips, Phys. Rev. B **67**, 104204 (2003).
[77]J. C. Maxwell, Philos. Mag. **27**, 294 (1864).
[78]M. Bauchy, M. Micoulaut, M. Celino, M. Boero, S. Le Roux, and C. Massobrio, Phys. Rev. B **83**, 054201 (2011).
[79]M. Micoulaut, C. Otjacques, J.-Y. Raty, and C. Bichara, Phys. Rev. B **81**, 174206 (2010).
[80]J. C. Mauro, P. K. Gupta, and R. J. Loucks, J. Chem. Phys. **130**, 234503 (2009).
[81]J. C. Mauro, R. J. Loucks, and P. K. Gupta, J. Phys. Chem. A **111**, 7957 (2007).
[82]C. A. Angell, B. E. Richards, and V. Velikov, J. Phys.: Condens. Matter **11**, A75 (1999).
[83]M. Smedskjaer, J. C. Mauro, R. E. Youngman, C. L. Hogue, M. Potuzak, and Y. Yue, J. Phys. Chem. B **115**, 12930 (2011).
[84]M. M. Smedskjaer, J. C. Mauro, and Y. Yue, Phys. Rev. Lett. **105**, 115503 (2010).
[85]K. Trachenko, M. T. Dove, V. Brazhkin, and F. S. El'kin, Phys. Rev. Lett. **93**, 135502 (2004).
[86]K. Trachenko and M. T. Dove, Phys. Rev. B **67**, 212203 (2003).
[87]K. Trachenko and M. T. Dove, J. Phys.: Condens. Matter **14**, 1143 (2002).
[88]M. F. Thorpe, D. J. Jacobs, M. V. Chubynsky, and J. C. Phillips, J. Non-Cryst. Solids **266-269**, 859 (2000).
[89]J. Barré, A. R. Bishop, T. Lookman, and A. Saxena, Phys. Rev. Lett. **94**, 208701 (2005).
[90]M. V. Chubynsky, M. A. Brière, and N. Mousseau, Phys. Rev. E **74**, 016116 (2006).
[91]D. Selvenathan, W. Bresser, and P. Boolchand, Solid State Commun. **111**, 619 (1999).
[92]S. Bhosle, K. Gunasekera, P. Boolchand, and M. Micoulaut, Int. J. Appl. Glass Sci. **3**, 205 (2012).
[93]K. Gunasekara, S. Bhosle, P. Boolchand, and M. Micoulaut, J. Chem. Phys. **139**, 164511 (2013).
[94]M. Bauchy and M. Micoulaut, Nat. Commun. **6**, 6398 (2015).